Structures and phase diagrams of N2 and CO to 13 GPa by xray diffraction

R. L. Mills, Bart Olinger, and D. T. Cromer

Articles you may be interested in

X-ray diffraction measurements of Mo melting to 119 GPa and the high pressure phase diagram
J. Chem. Phys. **130**, 124509 (2009); 10.1063/1.3082030

Compression of polyhedral graphite up to 43 GPa and x-ray diffraction study on elasticity and stability of the graphite phase
Appl. Phys. Lett. **84**, 5112 (2004); 10.1063/1.1763641

Crystal structures of N2O to 12 GPa by xray diffraction
J. Chem. Phys. **95**, 5392 (1991); 10.1063/1.461655

High pressure xray diffraction studies on solid N2 up to 43.9 GPa
J. Chem. Phys. **93**, 8968 (1990); 10.1063/1.459236

Structures and transitions in solid O2 to 13 GPa at 298 K by xray diffraction
J. Chem. Phys. **81**, 5068 (1984); 10.1063/1.447495

Structures and phase diagrams of N₂ and CO to 13 GPa by x-ray diffraction

R. L. Mills, Bart Olinger, and D. T. Cromer

University of California and Los Alamos National Laboratory, Los Alamos, New Mexico 87545

The structures and phase transitions of N₂ and CO were studied by powder x-ray diffraction from 100 to 300 K and 4 to 13 GPa. Three solid phases, β, δ, and ε, were observed in each material. The known β and δ solids were confirmed to have hexagonal space group $P6_3/mmc$ and cubic space group $Pm3n$, respectively. From refinements using photographic x-ray intensities, the new ε-N₂ and ε-CO structures were determined to be rhombohedral $R\bar{3}c$. There are eight ordered molecules in the ε-N₂ unit cell with $a = 5.928$ Å and $\alpha = 85.14°$ at 110 K and 7.8 GPa, and eight ordered molecules in the ε-CO unit cell with $a = 6.059$ Å and $\alpha = 85.73°$ at 100 K and 5.5 GPa. The CO molecules are randomly oriented head to tail. The δ–ε transition takes place through an ordering and small displacement of the N₂ and CO molecules, accompanied by a slight extension of the lattice along a cube diagonal. Molar volumes are presented over an expanded P-T region. Recent theoretical calculations using lattice energies, molecular dynamics, and symmetry correlations correctly predict features in the N₂ and CO phase diagrams.

INTRODUCTION

When compressed, many solids undergo structural phase transitions, the study of which is one of the most active areas of experimental and theoretical high-pressure research. With the advent of diamond cells, it is now possible to observe such transitions through changes in molecular spectra and x-ray diffraction at static pressures approaching 100 GPa (1 Mbar). Recent advances have also been made in computer modeling of transforming systems at high pressure. Results obtained with these new techniques have contributed to a better understanding of solid state physics, which underlies the important field of materials science.

Because they are relatively simple to treat theoretically, solidified gases made up of first-row elements are of current interest. In this group of materials, nitrogen and carbon monoxide constitute a unique pair of molecules with almost identical charges and masses. By studying N₂ and CO under pressure, we can gain information about the way subtle differences in intermolecular interactions affect physical and chemical behavior.

The phase diagrams of N₂ and CO, as determined from P-V-T measurements,[1–4] Raman scattering,[5–10] x-ray diffraction,[11–17] NMR,[18] and theoretical calculations[19–28] are shown schematically in Fig. 1. In the P-T domain of Fig. 1(a), solid nitrogen exists in at least six crystal forms: ordered cubic[29] α-N₂ (space group Pa3); disordered hexagonal[16,30,31] β-N₂ ($P6_3/mmc$); ordered tetragonal[11,12] γ-N₂ ($P4_2/mnm$); disordered cubic[6,14,17] δ-N₂ ($Pm3n$); ε-N₂ [formerly called[10] δ(LT1)-N₂, and probably rhombohedral $R\bar{3}c$]; and ζ-N₂ [formerly called[10] δ(LT2)-N₂, and possibly rhombohedral $R3c$]. The phase diagram for CO in Fig. 1(b) shows four analogous phases: ordered primitive cubic[32,33] α-CO ($P2_13$); disordered hexagonal[15] β-CO ($P6_3/mmc$); δ-CO (probably disordered cubic[8] $Pm3n$); and ε-CO (possibly rhombohedral[8] $R3c$). Measurements on CO extend only to about 10 GPa.

As shown in Fig. 1, the melting curves for N₂ and CO are almost identical. Also, both the α–β transition line (plus its γ–β extension) and the β–δ transition line for N₂ approach the respective lines for CO with increasing pressure and temperature. Slight variations in space groups between corresponding phases in N₂ and CO arise because CO is heteronuclear and, unlike N₂, can exhibit a slight asymmetry on lattice sites.[3,4]
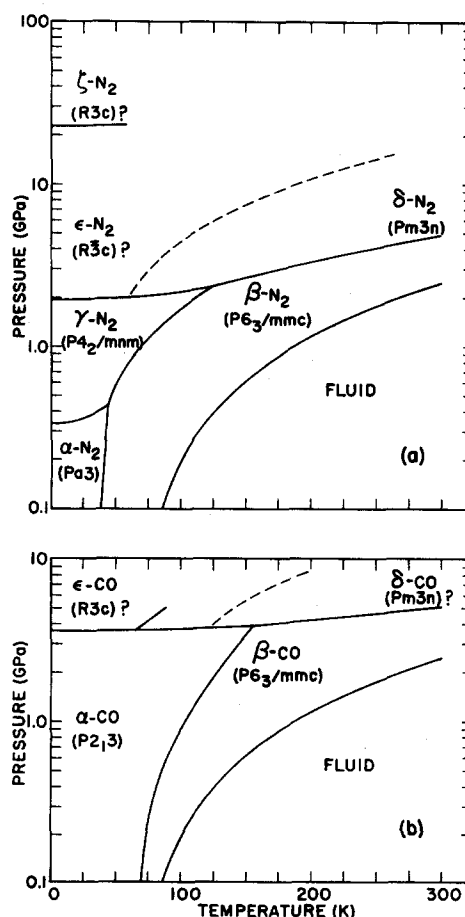

FIG. 1. Pressure-temperature diagrams showing fluid and solid phases with space groups in parentheses for (a) N₂ and (b) CO. Dashed lines are present results; tentative space groups for δ-CO and ε-N₂ are confirmed by the present study.
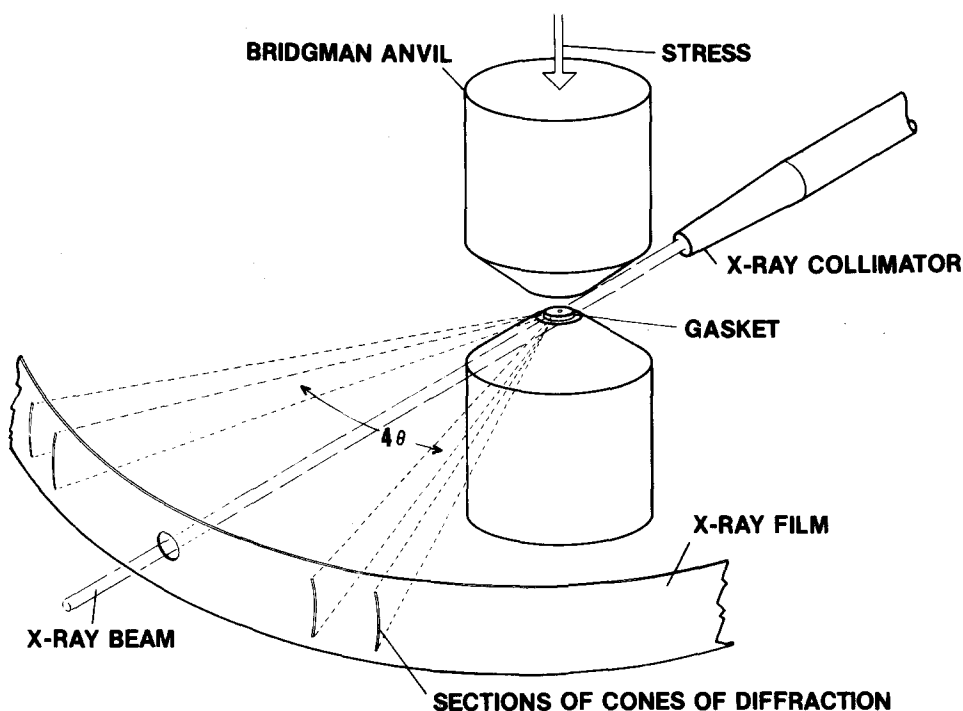
FIG. 2. Schematic diagram of the apparatus.

One noticeable difference between Figs. 1(a) and 1(b) is that no γ phase exists in CO. The electric quadrupole–quadrupole interaction, which is mainly responsible for the ordered cubic α structure, is much larger[35] in CO and stabilizes this structure to higher pressure. In N₂, on the other hand, the more efficient packing of ellipsoidal molecules on a tetragonal lattice[19] overrides the quadrupolar effect near 0.4 GPa and leads to the γ phase. It has been estimated[19] that a γ phase in CO would be favored over the α phase at pressures above about 4.8 GPa, but a transition to ϵ-CO intervenes at a slightly lower pressure.[8]

Another striking difference, not evident in Fig. 1, is that CO at room temperature becomes chemically unstable near 5 GPa and forms a yellow solid that can be recovered at zero pressure.[8,9] Analyses are underway in this Laboratory to characterize the newly synthesized CO solid product. Molecular nitrogen, on the other hand, was recently observed[36,37] up to at least 160 GPa. This finding conflicts with the prediction[38] of a transition to a metallic state near 80 GPa.

The present x-ray diffraction study was carried out to confirm the structures of N₂ and CO that have been inferred from Raman measurements and theoretical calculations, and to determine the phase diagrams and extend them to higher pressures. A preliminary account of the results on CO has already appeared.[9]

EXPERIMENTAL

Liquid N₂ or CO, with powdered NaF for pressure measurement, was trapped between two tungsten–carbide anvils in a 0.5 mm diam hole in the center of a 0.5 mm thick, 2.5 mm diam Be disk. We used a modification of the indium-dam loading technique, developed earlier[39] for diamond-anvil cells. In the experimental setup, shown in Fig. 2, the lower anvil was supported by tension rods while the upper

one was driven by a hydraulic ram. We directed a collimated beam of Cu $K\alpha$ x-rays radially through the Be disk, and recorded the diffracted radiation on film in a 114.6 mm diam powder camera surrounding the sample.

The sample was cooled by circulating liquid N₂ through hollow platens holding the anvils. We measured and controlled the temperature using the output from a copper–constantan thermocouple attached to the rim of the Be gasket. The temperature difference from the center to the edge of the gasket, when compressed between the anvils, was measured to be no greater than 1 K.

We determined the cell pressure from in situ NaF, used as a marker. The NaF relative volume is known as a function of pressure from shock-wave data and ultrasound speeds.[40] Values at 298 K up to 13 GPa in steps of 1 GPa are listed in Table I. We measured the volume of NaF from its (200) and

TABLE I. Cell constant and relative volume of sodium fluoride at 298 K as a function of pressure.ᵃ

P (GPa)	a (Å)	V/V_0
0.0	4.634	1.000
1.0	4.603	0.980
2.0	4.575	0.962
3.0	4.549	0.946
4.0	4.525	0.931
5.0	4.503	0.917
6.0	4.482	0.905
7.0	4.463	0.893
8.0	4.445	0.882
9.0	4.427	0.872
10.0	4.411	0.862
11.0	4.395	0.853
12.0	4.380	0.844
13.0	4.366	0.836

ᵃ Based on shock-wave compression and sound-speed data of Ref. 40.

TABLE II. Calculated and observed x-ray powder patterns for ε-N₂ at 7.8 GPa and 110 K.

hkl[a]	d_{obs}[b]	d_{calc}	I_{obs}	I_{calc}[c]	I_{calc}[c]
(hex)	(Å)	(Å)		model 1	model 2
012	...	4.337	0	0.0	0.6
110	...	4.010	0	0.4	0.5
202	2.939	2.944	50	45.5	77.7
113	2.713	2.720	100	72.6	100.0
104	2.585	2.578	20	28.8	46.3
211	2.541	2.555	80	100.0	87.6
122	2.374	2.373	40	92.4	60.1
300	2.316	2.315	20	17.2	18.2
024	2.167	2.168	10	20.8	0.0
220	d	2.005	d	9.1	0.0
214	d	1.907	d	1.1	0.0
131	d	1.898	d	2.9	0.1
006	...	1.851	0	2.6	1.9
312	...	1.820	0	0.1	0.0
223	d	1.763	d	0.3	0.2
125	d	1.700	d	0.8	6.1
116	d	1.680	d	0.0	4.8
042	...	1.657	0	1.4	2.3
134	1.577	1.583	10	5.4	2.7
321		1.577		4.0	2.6

[a] Hexagonal indexing is used for ease of fitting.
[b] Cell constants determined by least-squares fit are $a = 8.020 \pm 0.012$ Å, $c = 11.104 \pm 0.029$ Å, $c/a = 1.38$.
[c] Model 1 is for space group $R\bar{3}c$ with ordered molecules and model 2 is for spherically disordered molecules, as described in the text.
[d] Possible reflection masked by strong line from Be gasket.

TABLE III. Calculated and observed x-ray powder patterns for ε-CO at 5.5 GPa and 100 K.

hkl[a]	d_{obs}[b]	d_{calc}	I_{obs}	I_{calc}[c]	I_{calc}[c]
(hex)	(Å)	(Å)		model 1	model 2
012	...	4.418	0	0.0	4.3
110	...	4.122	0	0.4	0.2
202	3.014	3.014	70	44.2	48.6
113	2.770	2.774	70	70.8	71.5
211	2.662	2.624	100	100.0	100.0
104		2.617		26.9	16.1
122	2.433	2.433	80	91.6	67.5
300	2.381	2.380	10	17.5	40.6
024	2.207	2.209	20	20.6	9.9
220	...	2.061	0	9.1	2.7
131	d	1.950	d	3.0	10.4
214	d	1.947	d	0.9	1.7
006	...	1.875	0	2.8	0.3
312	...	1.868	0	0.1	1.9
223	...	1.806	0	0.3	1.3
125	d	1.728	d	0.9	0.4
116	d	1.707	d	0.0	3.3
042	d	1.701	d	1.6	2.9
321	1.622	1.621	10	4.4	7.1
134		1.619		5.5	7.0
232	...	1.573	0	0.5	4.7
140	1.558	1.558	10	11.0	8.7

[a] Hexagonal indexing is used for ease of fitting.
[b] Cell constants determined by least-squares fit are $a = 8.244 \pm 0.004$ Å, $c = 11.250 \pm 0.010$ Å, $c/a = 1.36$.
[c] Model 1 is for space group $R\bar{3}c$ and model 2 is for $R3c$ as described in the text.
[d] Possible reflection masked by strong line from Be gasket.

(220) x-ray diffraction lines, which were readily discernable from the specimen pattern. Below 298 K, the pressure at temperature T was calculated from the NaF pressures in Table I by subtracting the thermal pressure difference

$$\Delta P = (\alpha_P/\beta_T)\Delta T = 4.5 \times 10^{-3}(298-T)\text{GPa}, \qquad (1)$$

where α_P is the isobaric thermal expansion coefficient in K^{-1}, β_T is the isothermal compressibility coefficient in GPa^{-1}, and ΔT and T are in K. We assume that the ratio α_P/β_T for NaF is constant over our pressure-temperature range.[41] Raman and x-ray measurements on N₂ and CO have also been made in diamond cells, where the pressure was determined by ruby fluorescence.[42] This pressure scale has been established by normalizing the ruby R_1 line shift to the compression of NaCl measured by x-ray diffraction.[43] The correlation was made using the Mie–Grüneisen equation with ambient thermodynamic quantities.[43] If, instead, the compression of NaCl from shock-wave measurements[40] had been used, then ruby pressures would be consistent with the present NaF shock-wave pressures. We find, however, that our NaF-based pressures are higher than ruby-based pressures, for example, by 3% at 10 GPa. In comparing earlier diamond-cell measurements with our present data, we have made appropriate pressure shifts.

Diffraction patterns from three structures were observed in both N₂ and CO during the course of our study from 100 to 300 K and 4 to 13 GPa. Two of the structures, β and δ, were already known or suspected to have space group $P6_3/mmc$ and $Pm3n$, respectively (see Fig. 1). The new structure is that of the ϵ phase. In Table II, we show an

observed high-pressure, low-temperature diffraction pattern for ε-N₂ and, in Table III, one for ε-CO. Tables IV and V list all of our observations on N₂ and CO, respectively, including: the temperature, pressure, structure, lattice parameters, and molar volume.

DISCUSSION

β structure

The structure of β-N₂ at high pressure is known from single-crystal[13,16] and powder[17] x-ray diffraction to be disordered hexagonal close packed with space group $P6_3/mmc$, which is the same structure reported at zero pressure.[30] Although we have not included cell constants for β-N₂ in Table IV, our observations are consistent with the previous findings.[13,16,17,30]

New data for β-CO are presented in Table V at 200 and 300 K up to 5.2 GPa. Again the structure is $P6_3/mmc$ and is the same as that reported previously[15] at 2.7 and 3.6 GPa.

δ structure

From single-crystal[14] and powder[17] x-ray diffraction, the structure of δ-N₂ was reported to be disordered cubic with space group $Pm3n$, as shown in Fig. 3 on the left-hand side. The δ phase had been discovered earlier[6] from Raman spectra which exhibited a curious splitting in the stretching-mode frequency. A similar splitting was recently observed near 5.0 GPa and 297 K in a Raman study[8] of solid CO, from which it was inferred that a δ phase with space group $Pm3n$ also exists in CO. Our powder x-ray data for δ-CO, summar-

TABLE IV. Summary of N_2 x-ray data with standard deviations shown in parentheses.

Run	T (K)	a_{NaF} (Å)	P (GPa)	Phase	a (Å)	c (Å)	V (cm³/mol)
6–3	300	4.468	6.7	δ	6.050		16.67
		(0.002)	(0.1)		(0.006)		(0.05)
6–4	110	4.461	6.3	ϵ	8.140	11.34	16.33
		(0.002)	(0.1)		(0.022)	(0.066)	(0.18)
6–5	300	4.453	7.5	δ	5.998		16.24
		(0.001)	(0.1)		(0.007)		(0.06)
6–6	110	4.455	6.6	ϵ	8.128	11.272	16.18
		(0.000)	(0.0)		(0.014)	(0.030)	(0.10)
6–7	140	4.444	7.3	δ	5.952		15.88
		(0.002)	(0.2)		(0.001)		(0.01)
				ϵ	8.075	11.183	15.85
					(0.014)	(0.031)	(0.10)
6–8	150	4.444	7.5	δ	5.955		15.90
		(0.002)	(0.2)		(0.002)		(0.01)
				ϵ	8.082	11.170	15.86
					(0.009)	(0.035)	(0.09)
6–9	155	4.441	7.6	δ	5.951		15.86
		(0.002)	(0.1)		(0.008)		(0.06)
				ϵ	8.052	11.258	15.86
					(0.005)	(0.017)	(0.04)
6–10	170	4.437	7.9	δ	5.956		15.91
		(0.000)	(0.0)		(0.003)		(0.02)
6–11	130	4.491	5.6	δ	6.131		17.35
		(0.003)	(0.2)		(0.007)		(0.06)
7–7	110	4.478	5.4	ϵ	8.208	11.362	16.63
		(0.002)	(0.1)		(0.053)	(0.137)	(0.41)
7–8	110	4.470	5.8	ϵ	8.145	11.318	16.32
		(0.001)	(0.1)		(0.039)	(0.124)	(0.34)
7–9	110	4.463	6.2	ϵ	8.119	11.332	16.23
		(0.000)	(0.0)		(0.002)	(0.011)	(0.02)
7–10	110	4.446	7.1	ϵ	8.057	11.213	15.82
		(0.002)	(0.1)		(0.011)	(0.022)	(0.07)
7–11	110	4.437	7.5	ϵ	8.012	11.160	15.57
		(0.002)	(0.1)		(0.016)	(0.030)	(0.10)
7–12	110	4.435	7.8	ϵ	8.020	11.104	15.52
		(0.002)	(0.1)		(0.012)	(0.029)	(0.09)
7–13	110	4.434	7.8	ϵ	8.015	11.066	15.45
		(0.000)	(0.0)		(0.019)	(0.047)	(0.14)
7–14	110	4.433	7.9	ϵ	8.026	11.096	15.53
		(0.001)	(0.1)		(0.022)	(0.047)	(0.15)
7–15	110	4.425	8.3	ϵ	7.992	11.066	15.36
		(0.001)	(0.1)		(0.019)	(0.045)	(0.14)
7–16	110	4.418	8.7	ϵ	7.930	11.053	15.10
		(0.001)	(0.1)		(0.010)	(0.025)	(0.07)
7–17	110	4.414	8.9	ϵ	7.924	11.048	15.07
		(0.002)	(0.1)		(0.008)	(0.024)	(0.06)
7–18	110	4.413	9.0	ϵ	7.904	11.044	14.99
		(0.001)	(0.1)		(0.011)	(0.028)	(0.08)
7–19	110	4.402	9.8	ϵ	7.859	11.029	14.80
		(0.000)	(0.0)		(0.013)	(0.031)	(0.09)
7–20	300	4.483	11.8	δ	5.790		14.61
		(0.002)	(0.1)		(0.008)		(0.06)
7–21	195	4.375	11.9	ϵ	7.801	10.823	14.31
		(0.001)	(0.1)		(0.019)	(0.070)	(0.16)
7–22	250	4.372	12.4	$\delta + \epsilon$	5.753		14.33
		(0.000)	(0.0)		(0.017)		(0.12)
7–23	220	4.373	12.2	$\delta + \epsilon$	5.739		14.23
		(0.000)	(0.0)		(0.010)		(0.07)
					7.770	10.821	14.20
					(0.010)	(0.015)	(0.06)
7–24	235	4.369	12.5	δ	5.738		14.22
		(0.000)	(0.0)		(0.011)		(0.08)
7–25	235	4.373	12.2	δ	5.742		14.25
		(0.001)	(0.1)		(0.011)		(0.08)
7–26	130	4.366	12.2	ϵ	7.746	10.865	14.17
		(0.001)	(0.1)		(0.014)	(0.021)	(0.08)
7–27	300	4.367	12.9	δ	5.742		14.25
		(0.002)	(0.2)		(0.011)		(0.08)

TABLE IV. (*continued*).

Run	T (K)	a_{NaF} (Å)	P (GPa)	Phase	a (Å)	c (Å)	V (cm³/mol)
7–28	270	4.366 (0.001)	12.9 (0.1)	δ	5.740 (0.008)		14.23 (0.06)
7–29	250	4.367 (0.002)	12.7 (0.2)	δ	5.743 (0.005)		14.26 (0.04)
7–30	225	4.369 (0.001)	12.5 (0.1)	δ + ε			
7–31	245	4.363 (0.001)	13.0 (0.1)	δ	5.740 (0.010)		14.24 (0.07)
7–32	235	4.366 (0.001)	12.7 (0.1)	δ	5.743 (0.001)		14.26 (0.01)
7–33	230	4.364 (0.001)	12.9 (0.1)	δ	5.736 (0.003)		14.21 (0.02)
7–34	225	4.362 (0.002)	13.0 (0.2)	δ + ε	5.740 (0.001)		14.24 (0.01)
					7.745 (0.016)	10.813 (0.016)	14.10 (0.08)
7–35	225	4.369 (0.002)	12.5 (0.2)	δ + ε	5.744 (0.004)		14.27 (0.03)
					7.760 (0.013)	10.824 (0.039)	14.16 (0.10)
7–36	235	4.377 (0.001)	11.9 (0.1)	δ	5.735 (0.003)		14.20 (0.02)
7–37	215	4.364 (0.000)	12.8 (0.0)	ε			
7–38	235	4.364 (0.001)	12.8 (0.1)	δ	5.737 (0.010)		14.21 (0.07)
7–39	300	4.363 (0.000)	13.2 (0.0)	δ	5.732 (0.002)		14.18 (0.01)
7–40	300	4.365 (0.000)	13.0 (0.0)	δ	5.738 (0.018)		14.22 (0.13)
7–41	210	4.363 (0.002)	12.8 (0.2)	ε	7.736 (0.009)	10.814 (0.021)	14.06 (0.006)
7–42	190	4.365 (0.001)	12.6 (0.1)	ε	7.743 (0.007)	10.798 (0.016)	14.07 (0.05)
7–43	175	4.365 (0.002)	12.6 (0.2)	ε	7.749 (0.008)	10.862 (0.024)	14.17 (0.06)
7–44	150	4.363 (0.002)	12.5 (0.2)	ε	7.739 (0.007)	10.848 (0.021)	14.12 (0.05)
7–45	130	4.362 (0.004)	12.5 (0.3)	ε	7.723 (0.009)	10.861 (0.026)	14.08 (0.07)
7–46	105	4.360 (0.002)	12.6 (0.2)	ε	7.724 (0.011)	10.899 (0.028)	14.13 (0.08)
7–47	300	4.360 (0.000)	13.5 (0.0)	δ	5.719 (0.021)		14.08 (0.15)

ized in Table V, are consistent with a cubic *Pm3n* lattice having eight disordered molecules in a unit cell of about 6 Å. The uncertainty in the space group for δ-CO, indicated in Fig. 1(b), is therefore removed.

ε structure

For ease in handling the fitting routines, we indexed the eight diffraction lines from rhombohedral ε-N₂ on the basis of a hexagonal cell with $a = 8.020 \pm 0.012$ Å and $c = 11.104 \pm 0.029$ Å, as shown in Table II. Systematic extinctions were consistent with space groups $R\,3c$ and $R\,\overline{3}c$. The molecular volume of ε-N₂ at 7.8 GPa and 110 K was estimated to be 25.9 Å³ from an extrapolation of δ-N₂ data, neglecting any volume change on transition. This gave an ε-N₂ unit cell on a hexagonal basis containing 24 molecules. We considered structures in which six of the molecules were accommodated by placing the 12 atoms in positions 0,0, ± z in one or the other of the above space groups. The remaining 18 molecules were arranged with 36 atoms distributed either

in two 18-fold general positions in $R\,3c$ or in one 36-fold general position in $R\,\overline{3}c$.

We used Busing's[44] WMIN program to locate and orient the 18-fold N₂ molecule, the potential parameters of which were taken from Mirsky.[45] The molecule was treated as a rigid body with internuclear distance held at 1.099 Å. The sixfold molecule was fixed while the 18-fold molecule was allowed to translate and rotate from an arbitrary starting position in space group $R\,3c$. Using Busing's mode 3 (Rosenbrock search),[44] we found an energy minimum when the center of the molecule moved to a position on the twofold axis of $R\,\overline{3}c$ at $x,x,1/4$. Thus we take as model 1 a structure described as having one N atom at 0, 0, 0.0495 and one at 0.2731, 0.2127, 0.2828 in $R\,\overline{3}c$ with a crystal energy of − 9.29 kcal/mol. The ε-N₂ structure, shown as rhombohedral on the right-hand side of Fig. 3, is ordered with closest interatomic distances N(1)–3N(2) of 2.73 and 2.80 Å.

Table II shows the observed and calculated powder patterns for ε-N₂. The agreement is quite satisfactory, consider-

TABLE V. Summary of CO x-ray data with standard deviations shown in parentheses.

Run	T (K)	a_{NaF} (Å)	P (GPa)	Phase	a (Å)	c (Å)	V (cm³/mol)
2–7	300	4.523 (0.001)	4.1 (0.1)	β	3.550 (0.007)	5.765 (0.018)	18.95 (0.13)
2–8	300	4.515 (0.001)	4.4 (0.0)	β	3.504 (0.011)	5.720 (0.028)	18.31 (0.20)
2–9	300	4.499 (0.000)	5.2 (0.0)	β	3.470	5.711	17.93
2–10	300	4.493 (0.002)	5.5 (0.1)	δ	6.136 (0.017)		17.39 (0.14)
2–11	300	4.491 (0.002)	5.5 (0.1)	δ	6.139 (0.023)		17.42 (0.19)
2–12	300	4.489 (0.001)	5.7 (0.1)	δ	6.116 (0.031)		17.22 (0.26)
2–13	300	4.499 (0.002)	5.2 (0.1)	δ	6.162		17.61
2–14	300	4.504 (0.001)	4.9 (0.1)	δ	6.181		17.78
2–15	300	4.512 (0.001)	4.6 (0.0)	δ	6.213		18.05
2–16	300	4.530 (0.002)	3.8 (0.1)	β	3.567	5.868	19.47
2–17	300	4.524 (0.003)	4.1 (0.2)	β	3.541	5.761	18.77
3–1	300	4.519 (0.001)	4.3 (0.1)	β	3.543 (0.002)	5.751 (0.003)	18.82 (0.03)
3–3	300	4.527 (0.000)	3.9 (0.0)	β	3.549 (0.019)	5.766 (0.030)	18.94 (0.30)
3–4	200	4.519 (0.000)	3.8 (0.0)	β	3.545 (0.000)	5.744 (0.001)	18.82 (0.00)
3–5	300	4.524 (0.001)	4.1 (0.1)	β	3.557 (0.005)	5.771 (0.009)	19.04 (0.08)
3–6	200	4.512 (0.001)	4.1 (0.1)	β	3.514 (0.009)	5.727 (0.016)	18.44 (0.15)
3–7	200	4.494 (0.001)	5.0 (0.1)	δ	6.137 (0.018)		17.40 (0.15)
3–8	140	4.496 (0.001)	4.7 (0.1)	δ	6.133 (0.003)		17.37 (0.03)
				ϵ	8.364 (0.013)	11.451 (0.023)	17.41 (0.09)
4–2	170	4.497 (0.002)	4.7 (0.1)	δ	6.158 (0.003)		17.58 (0.03)
4–3	170	4.458 (0.002)	6.7 (0.1)	δ	6.029 (0.008)		16.50 (0.07)
				ϵ	8.195 (0.016)	11.211 (0.033)	16.36 (0.10)
4–4	150	4.452	7.0	δ	6.022 (0.009)		16.44 (0.07)
4–5	150	4.451 (0.001)	7.0 (0.0)	δ	6.007 (0.011)		16.32 (0.10)
4–6	200	4.446 (0.002)	7.6 (0.1)	δ	6.001 (0.015)		16.27 (0.12)
5–2	100	4.450 (0.003)	6.9 (0.2)	ϵ	8.137 (0.005)	11.112 (0.012)	15.99 (0.04)
6–2	100	4.475 (0.000)	5.5 (0.0)	ϵ	8.244 (0.004)	11.250 (0.010)	16.62 (0.03)
7–3	145	4.508 (0.001)	4.1 (0.0)	δ	6.226 (0.010)		18.17 (0.08)
7–4	145	4.505 (0.002)	4.3 (0.1)	δ	6.201 (0.005)		17.95 (0.04)
7–5	145	4.484 (0.000)	5.3 (0.0)	δ	6.103 (0.010)		17.12 (0.08)
				ϵ	8.370 (0.005)	11.223 (0.014)	17.06 (0.05)

ing that only crude intensities could be obtained in this rather difficult experiment. Also shown in Table II are computed intensities for a model 2 with spherically disordered N_2 molecules centered at 0, 0, 0 and 0.243, 0.243, 0.250. In this model, the electron density is spherically distributed. The agreement is equally good, with the striking exception that the reflection at 024, which was clearly seen, is calculated to have zero intensity. We therefore dismiss model 2.
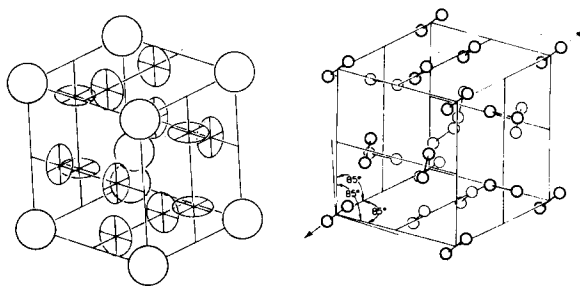
FIG. 3. Solid N₂ structures. Left-hand side, cubic δ-N₂ ($Pm3n$), showing molecules with spherical and disk shaped disorder; right-hand side, rhombohedral ϵ-N₂ ($R\bar{3}c$), showing ordered molecules and distortion of cubic cell.

The observed x-ray pattern of ϵ-CO in Table III is quite similar to that shown in Table II for ϵ-N₂. If the slightly asymmetric CO molecules were oriented with complete head-to-tail alignment, the ordered rhombohedral structure would be $R\,3c$ rather than $R\bar{3}c$. The following thermodynamic evidence, however, favors $R\bar{3}c$. In solid CO at zero pressure, the molecular axes become ordered at the β–α transition, while the heads and tails (C and O ends) stay almost randomly distributed. Calorimetric measurements[34,46] show that about 80% of the α-CO molecules are disordered head to tail and remain so[47,48] at temperatures well below the calculated dipolar ordering temperature[49] $T_c = 5$ K. The randomness is effectively frozen in at much higher temperatures. A recent dielectric study[50] on α-CO indicates that, even at 3.5 T_c, the reorientation rate is only 1 molecule/h.

A similar situation no doubt exists at higher temperatures and pressures where the internuclear axes in disordered δ-CO become ordered in ϵ-CO. At 100 K and 5.5 GPa, the molecules occupy only about 60% of their zero-pressure volume in α-CO, and one expects 180° head-to-tail flips to be extremely rare. We have, therefore, chosen as model 1 for ϵ-CO the probable configuration in which head-to-tail orientations of the molecules are randomly distributed. Unfortunately, the WMIN program could not be used to treat this $R\bar{3}c$ model for CO directly, and we were obliged to calculate x-ray intensities for a model similar to that of model 1 for N₂, but adjusted for the larger unit cell and larger bond length (1.127 Å) of CO, and with a scattering factor for x rays taken as the mean of that for C and O.

We were able, however, to use WMIN to minimize the energy of an ordered head-to-tail structure for CO in the $R\,3c$ space group. Two possibilities exist for this structure, most simply realized by flipping the molecule lying along 0, 0, z. Of the two structures produced by WMIN, one exhibited a rather short nonbonded 0–0 distance. The other orientation, with C(1) at 0, 0, 0.0501; O(1) at 0, 0, − 0.0501; C(2) at 0.2539, 0.2321, 0.2850; and O(2) at 0.2387, 0.2947, 0.1996, had reasonable nonbonded distances, and was chosen as model 2.

Table III shows the observed and calculated patterns for ϵ-CO. Again the agreement is good considering the nature of the experiment. The fit of both absolute and relative intensities, however, is more consistent for model 1 than for model 2. This supports our contention that, in the highly compressed solid, head-to-tail ordering by the weak dipolar in-

teraction between CO molecules does not occur to an appreciable extent. In CO, as in N₂, the observation of a reflection at 024 rules out a structure with spherically disordered molecules.

Mechanism of δ–ϵ transition

The hexagonal indices in Tables II and III all satisfy the relationship $-h + k + l = 3i$, where i is an integer, indicating that the lattice, which we indexed for convenience on a hexagonal basis, is truly rhombohedral. The rhombohedral unit cell contains eight ordered molecules and has cell constants $a = 5.928$ Å, $\alpha = 85.14°$ for ϵ-N₂ and $a = 6.059$ Å, $\alpha = 85.73°$ for ϵ-CO under our experimental P and T conditions. This cell, therefore, bears a close resemblence to that for cubic δ-N₂ which contains eight disordered molecules with $a \cong 6$ Å and $\alpha = 90°$. The δ–ϵ transition can be thought of as taking place through an ordering and small displacement of the N₂ molecules, accompanied by a slight extension of the lattice along the cube diagonal, resulting in a shift of less than 5° in the angle between axes. The δ-N₂ and ϵ-N₂ lattices are compared in Fig. 3. A similar mechanism can explain the δ-CO to ϵ-CO transition.

Phase diagrams

In eight of the x-ray photographs for N₂, listed in Table IV, diffraction patterns appeared from coexisting δ and ϵ phases. Assuming the corresponding P-T conditions gave equilibrium points on the δ–ϵ transition line, we have drawn the dashed curve in Fig. 1(a) to represent the new phase boundary. Unfortunately, our x-ray measurements did not extend to sufficiently high pressures and low temperatures to enter the ζ-N₂ phase, formerly called δ(LT2)-N₂, which was discovered[10] by Raman spectroscopy. Another unidentified phase of N₂ observed by Raman scattering[51] above about 20 GPa at room temperature was also out of reach. Recent Raman measurements[36,37] show that the phase diagram of molecular nitrogen extends up to at least 160 GPa.

Coexisting δ-CO and ϵ-CO were observed in three photographs, allowing us to draw the δ–ϵ transition line shown as the dashed curve in Fig. 1(b). This phase line does not agree with the short solid line which represents a transition observed by changes in lattice-mode Raman spectra.[9] More recent Raman data,[51] however, show a second transition in the vicinity of the dashed line. It is possible that the ϵ-CO domain lies only between the short solid and dashed lines and that a different, unidentified phase exists at lower temperatures.

In all of our experiments on CO above about 50 GPa at room temperature, the x-ray patterns faded with pressure and finally disappeared, suggesting that the crystalline samples underwent some sort of chemical change. A similar reaction was reported in earlier diamond-cell studies.[8,9] The CO phase diagram seems to be bounded at high pressure by a broadband that extends roughly from 5 GPa at 300 K to 12 GPa at 15 K. Above this band CO becomes chemically unstable and forms solid products that vary in color from light yellow to black and can be recovered at zero pressure. The exact composition of the products and the nature of the chemical reactions are still under investigation.[9]
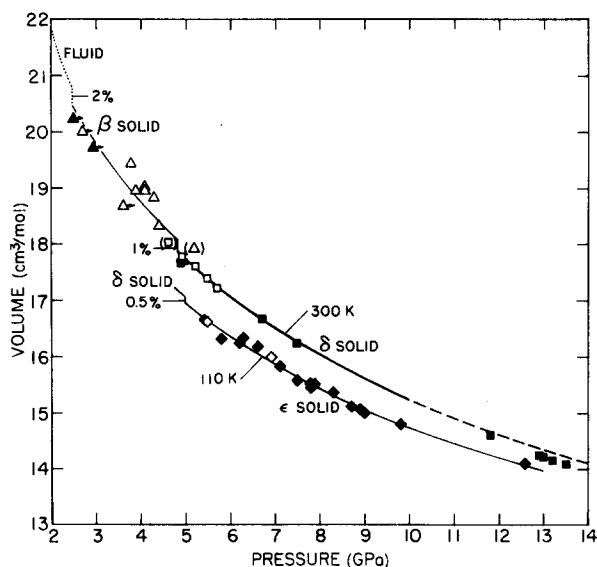
FIG. 4. Volume-pressure diagram of N_2 (closed symbol) at 110 and 300 K with CO data (open symbol) superimposed. Triangle, hexagonal β solid ($P6_3/mmc$); square, cubic δ solid ($Pm3n$); diamond, rhombohedral ϵ solid ($R\bar{3}c$), with ϵ-CO at 100 K; heavy solid line, Eqs. (2) and (5) Ref. 17, with dashed-line extrapolation; light solid line, visual guide; dotted line, Ref. 4; vertical line, transition in N_2, showing percent volume change; symbol with arrow, x-ray measurement in diamond cell, Refs. 13–16, showing shift to NaF pressure scale; symbol in parenthesis, nonequilibrium point.
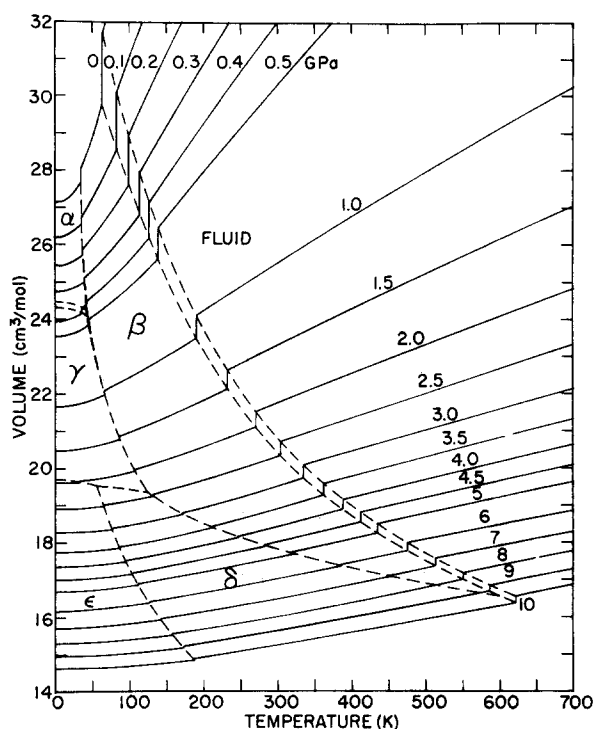

FIG. 5. Volume-temperature diagram of N_2 incorporating extensive literature data, present results, and unpublished work at high temperature, Ref. 52. Dashed line, phase boundary; solid line, isobar, showing volume discontinuity at transition.

Molar volumes

Molar volumes in the β, δ, and ϵ phases are plotted in Fig. 4 at 300 and 110 K. Within experimental error, the solid symbols for N_2 coincide with the open symbols for CO, although scatter in the β-CO volumes at 300 K is rather large. Nevertheless, the agreement between the present powder data and previous single-crystal results in diamond cells, properly shifted to the NaF pressure scale, is satisfactory. It should be noted that the volume discontinuities, shown in the curves of Fig. 4, represent phase transitions in N_2 only. Transitions in CO would appear at different pressures [see Figs. 1(a) and 1(b)].

In Fig. 4 the heavy solid curve represents an equation of state (EOS) for δ-N_2 at 296 K, fitted to earlier powder x-ray data[17] and extrapolated as the dashed line. The extrapolation lies about 1% above our present volumes at 13 GPa. It is now posssible to refine and extend the EOS by incorporating the present data for δ-N_2. The result at room temperature from about 5 to 14 GPa is

$$\psi_s = 2.995 + 1.090\psi_p \quad \text{and} \quad V_0 = 0.840 \text{ cm}^3/\text{g}, \quad (2)$$

where

$$P = \psi_s\psi_p/V_0(\text{GPa})$$

and

$$V = V_0(\psi_s - \psi_p)/\psi_s(\text{cm}^3/\text{g})$$

with ψ_s being a shock velocity and ψ_p a particle velocity.

We have made a similar least-squares fit to the ϵ-N_2 volumes at 110 K from 5 to 13 GPa, giving

$$\psi_s = 1.488 + 1.338\psi_p \quad \text{and} \quad V_0 = 1.065 \text{ cm}^3/\text{g}. \quad (3)$$

By extrapolating δ-N_2 data down to 110 K in the pressure

region 7.5–8.0 GPa, we estimate that the volume decrease on transition from disordered δ-N_2 to ordered ϵ-N_2 is 0.5%.

We have combined the molar volumes of Table IV with extensive literature values at lower pressures to expand the V-T diagram for N_2, as shown in Fig. 5. The drawing is also based on extrapolations of previous data and on a recent determination of the N_2 melting curve near 650 K by Raman spectroscopy in a diamond cell.[52]

Comparison with theory

From lattice-energy calculations at 0 K, Kobashi *et al.*[22] predicted a pressure-induced transition at 4 GPa from γ-N_2 ($P4_2/mnm$) to a new structure, termed ϵ-N_2, with space group $R\bar{3}m$. The volume change, $\Delta V(\gamma-\epsilon)$, was computed to be about 1%. LeSar and Gordon[27] published 0 K calculations using an electron-gas model which also gave a transition to $R\bar{3}m$, but at 10 GPa. These pioneering studies,[22,27] however, must be discounted because the $R\bar{3}m$ structure conflicts with known Raman spectra.[6,14]

A calculation that minimized the potential energy of a distorted $Pm3n$ lattice was carried out by Chandrasekharan *et al.*[24] They observed a low-temperature transition from $P4_2/mnm$ to $R\bar{3}c$ at 1.9 GPa, which is more consistent with experiment.[6,14] A second transition to $R\bar{3}m$ was predicted at 6.8 GPa. LeSar[28] used an improved electron-gas model with damped dispersion to predict a 0 K transition from γ-N_2 to ϵ-N_2 ($R\bar{3}c$) at 2 GPa, in complete agreement with Raman measurements.[6,14] Moreover, the atomic positions in ϵ-N_2, calculated by LeSar for 8 GPa and 0 K, agree almost exactly with those from the present x-ray study. The discrepancy is ± 0.02 Å for the center and corner molecules, where both

studies assumed the same symmetry, and ± 0.09 Å for the face molecules, where LeSar assumed a symmetry with two parallel molecules, and we relaxed this symmetry.

In recent Raman experiments at 15 K, Schiferl et al.[10] demonstrated by a comprehensive study of correlation diagrams that ϵ-N_2 has the likely structure $R\bar{3}c$, which we report here. The phase observed near 27 GPa and 15 K was shown[10] by similar symmetry arguments to have possible space group $R3c$. Unfortunately, we could not attain the P and T conditions necessary to enter this phase in the present x-ray experiments.

The earliest theoretical study of δ-N_2 was carried out by Klein et al.[25] who applied molecular dynamics (MD) to a system of 512 interacting molecules. They found a close resemblance to γ-O_2, which has the same $Pm3n$ structure, and were able to calculate translational and rotational spectra associated with the two types of disordered molecules. Using an improved MD technique, Nosé and Klein[26] observed two transitions on cooling δ-N_2 at 7 GPa. The first occurred at 230 K and produced cubic space group $I2_13$ in which the disk-shaped disordered molecules (see Fig. 3) were aligned parallel to the cube axes. In a second transition at 140 K, the spherically disordered molecules of $Pm3n$ became oriented along the trigonal direction. This gave a shearing distortion of 3° from the cubic axes, resulting in $R3c$ symmetry and an overall volume change of less than 1%.

In comparing our experimental observations with the MD calculations, we find that the δ–ϵ transition in N_2 at 7 GPa does indeed occur at 140 K, giving $R\bar{3}c$ with a cubic distortion of 5° and a $\Delta V(\delta$–$\epsilon)$ of 0.5%. The structure change, however, appears to take place in one step, and, while the spherically disordered molecules orient along a former cube diagonal, the disk molecules do not align parallel to the cube axes. As Fig. 3 shows, these molecules are fixed at unique angles, similar to those described by LeSar.[28] It is quite encouraging that recent theoretical calculations using different approaches[10,24,26,28] give such accurate predictions.

ACKNOWLEDGMENTS

[1] C. A. Swenson, J. Chem. Phys. 23, 1963 (1955).

[2] J. W. Stewart, J. Phys. Chem. Solids 1, 146 (1956).

[3] R. Stevenson, J. Chem. Phys. 27, 673 (1957).

[4] R. L. Mills, D. H. Liebenberg, and J. C. Bronson, J. Chem. Phys. 63, 4026 (1975).

[5] M. M. Thiery, D. Fabre, M. Jean-Louise, and H. Vu, J. Chem. Phys. 59, 4559 (1973).

[6] R. LeSar, S. A. Ekberg, L. H. Jones, R. L. Mills, L. A. Schwalbe, and D. Schiferl, Solid State Commun. 32, 131 (1979).

[7] S. Buchsbaum, R. L. Mills, and D. Schiferl, J. Phys. Chem. 88, 2522 (1984).

[8] A. I. Katz, D. Schiferl, and R. L. Mills, J. Phys. Chem. 88, 3176 (1984).

[9] R. L. Mills, D. Schiferl, A. I. Katz, and B. W. Olinger, J. Phys. (Paris) 45, C8-187 (1984).

[10] D. Schiferl, S. Buchsbaum, and R. L. Mills, J. Phys. Chem. 89, 2324 (1985).

[11] R. L. Mills and A. F. Schuch, Phys. Rev. Lett. 23, 1154 (1969).

[12] A. F. Schuch and R. L. Mills, J. Chem. Phys. 52, 6000 (1970).

[13] D. Schiferl, D. T. Cromer, and R. L. Mills, High Temp. High Pressure 10, 493 (1978).

[14] D. T. Cromer, R. L. Mills, D. Schiferl, and L. A. Schwalbe, Acta Crystallogr. Sect. B 37, 8 (1981).

[15] D. T. Cromer, D. Schiferl, R. LeSar, and R. L. Mills, Acta Crystallogr. Sect. C 39, 1146 (1983).

[16] D. Schiferl, D. T. Cromer, R. R. Ryan, A. C. Larson, R. LeSar, and R. L. Mills, Acta Crystallogr. Sect. C 39, 1151 (1983).

[17] B. Olinger, J. Chem. Phys. 80, 1309 (1984).

[18] E. Fukushima, A. A. V. Gibson, and T. A. Scott, J. Low Temp. Phys. 28, 157 (1977).

[19] J. C. Raich and R. L. Mills, J. Chem. Phys. 55, 1811 (1971).

[20] G. I. Kerley and J. Abdallah, Jr., J. Chem. Phys. 73, 5337 (1980).

[21] K. Kobashi and T. Kihara, J. Chem. Phys. 72, 378 (1980).

[22] K. Kobashi, A. A. Helmy, R. D. Etters, and I. L. Spain, Phys. Rev. B 26, 5996 (1982).

[23] R. D. Etters and A. Helmy, Phys. Rev. B 27, 6439 (1983).

[24] V. Chandrasekharan, R. D. Etters, and K. Kobashi, Phys. Rev. B 28, 1095 (1983).

[25] M. L. Klein, D. Levesque, and J. J. Weis, Can. J. Phys. 59, 530 (1981).

[26] S. Nosé and M. L. Klein, Phys. Rev. Lett. 50, 1207 (1983).

[27] R. LeSar and R. G. Gordon, J. Chem. Phys. 78, 4991 (1983).

[28] R. LeSar, J. Chem. Phys. 81, 5004 (1984).

[29] J. A. Venables and C. A. English, Acta Crystallogr. Sect. B 30, 929 (1974).

[30] W. E. Streib, T. H. Jordan, and W. N. Lipscomb, J. Chem. Phys. 37, 2962 (1962).

[31] B. M. Powell, G. Dolling, and H. F. Nieman, J. Chem. Phys. 79, 982 (1983).

[32] A. Anderson, T. S. Sun, and M. C. A. Donkersloot, Can. J. Phys. 48, 2265 (1970).

[33] B. O. Hall and H. M. James, Phys. Rev. B 13, 3590 (1976).

[34] J. O. Clayton and W. F. Giauque, J. Am. Chem. Soc. 54, 2610 (1932).

[35] D. E. Stogryn and A. P. Stogryn, Mol. Phys. 11, 371 (1966).

[36] R. Reichlin, D. Schiferl, S. Martin, C. Vanderborgh, and R. L. Mills, Phys. Rev. Lett. 55, 1464 (1985).

[37] R. J. Hemley, H. K. Mao, and P. M. Bell (private communication).

[38] A. K. McMahan and R. LeSar, Phys. Rev. Lett. 54, 1929 (1985).

[39] R. L. Mills, D. H. Liebenberg, J. C. Bronson, and L. C. Schmidt, Rev. Sci. Instrum. 51, 891 (1980).

[40] W. J. Carter, High Temp. High Pressure 5, 313 (1973). The input values listed in the reference are correct, but the values of isothermal compression are incorrect.

[41] B. Olinger and J. C. Jamieson, High Temp. High Pressure 5, 123 (1973).

[42] J. D. Barnett, S. Block, and G. J. Piermarini, Rev. Sci. Instrum. 44, 1 (1973).

[43] D. L. Decker, J. Appl. Phys. 42, 3239 (1971).

[44] W. R. Busing, Oak Ridge National Laboratory Report ORNL-5747 (1981).

[45] K. Mirsky, in Computing in Crystallography, edited by H. van Konigveldt and G. S. Bassi (Delft University, Delft, 1978).

[46] R. W. Blue and W. F. Giauque, J. Am. Chem. Soc. 57, 991 (1935).

[47] E. K. Gill and J. A. Morrison, J. Chem. Phys. 45, 1585 (1966).

[48] J. C. Burford and G. M. Graham, Can. J. Phys. 47, 23 (1969).

[49] M. W. Melhuish and R. L. Scott, J. Phys. Chem. 68, 2301 (1964).

[50] K. R. Nary, P. L. Kuhns, and M. S. Conradi, Phys. Rev. B 26, 3370 (1982).

[51] A. I. Katz, D. Schiferl, and R. L. Mills (unpublished results).

[52] D. Schiferl (unpublished results).